Large current ion beam polishing and characterization of mechanically finished titanium alloy (Ti6Al4V) surface

Guangxue Zhou[a], Yongchen Bi[a], Yuanhang Ma[a], Langping Wang[a,*], Xiaofeng Wang[a], Yonghao Yu [b,*], Andreas Mutzke [c]

[a]State Key Laboratory of Advanced Welding and Joining, Harbin Institute of Technology, Harbin 150001, P.R. China

[b]Academy of Fundamental and Interdisciplinary Science, Harbin Institute of Technology, Harbin 150001, P.R. China

[c]Max-Planck-Institut für Plasmaphysik, Wendelsteinstrasse 1, D-17491 Greifswald, Germany

* Corresponding author
Professor Langping Wang
E-mail addresses: aplpwang@hit.edu.cn.
Tel: +86-451-86418728
Fax: +86-451-86416186

Dr. Yonghao Yu
E-mail addresses: yhyu@hit.edu.cn

Submitted to: ***APPLIED SURFACE SCIENCE***

(With 14 figures)

ABSTRACT

Ti6Al4V samples with a surface roughness of about 0.2 μm were polished by a high fluence ion beam source, and influences of the ion current, energy and incident angle on the surface roughness of Ti6Al4V were studied. The as-polished surfaces were characterized by laser scanning confocal microscopy (LSCM), atomic force microscopy (AFM), grazing incidence X-ray diffraction (GIXRD) and X-ray photoelectron spectroscopy (XPS). The LSCM images revealed that the density of pits in the original surface decreased greatly after the ion polishing process. In addition, the surface roughness calculated from these images proved that the mean value reduced to 53 nm with an ion energy, current and incident angle of 600 eV, 130 mA and 75 °, respectively. The smoothing effect was also confirmed by the power spectral density (PSD) functions calculated from the AFM data. GIXRD patterns indicated that the Ti6Al4V samples mainly contain the hexagonal close packed (HCP) α-Ti, no recognizable peaks corresponding to the body centered cubic (BCC) β-Ti were observed. Furthermore, after the ion beam polishing process, the phase of all the as-polished samples kept steady. The XPS results revealed that C, O, Ti, Al and V were present in both the original as well as the polished samples. In addition, due to the highly reactive characteristics of Ti, Al and V elements, a higher signal for oxygen can also be observed on the outermost surface of the ion beam polished samples. The polishing process of Ti6Al4V surface bombarded by Ar ion beam is also simulated by binary collision approximation (BCA) code SDTrimSP, the effects of ion beam

energy and incident angle on the sputtering yield were investigated. The results showed that the sputtering yield of Ti, Al and V atoms increased almost linearly with the ion energy. However, as for the influence of ion incident angle, the sputtering yield first increased gradually from 0° and peaked at about 65°, then decreased rapidly because the incident angle is too large for Ar ion to penetrate into the surface of Ti6Al4V sample.

Keywords: Ion beam polishing, Roughness, Ti6Al4V, SDTrimSP

1. INTRODUCTION

Owing to their excellent properties, for examples, high strength-to-weight ratio, good corrosion resistance, excellent biocompatibility, as well as complete inertness to the body environment, titanium and its alloys have received considerably interest in biomedical implant applications from dental implants, bone fixation devices, artificial heart valves to parts for orthodontic surgery[1-6]. Although many types of titanium alloys are available, the titanium-aluminum-vanadium alloy (Ti6Al4V) is the most commonly used alloy, since its physical and mechanical properties are superior to those of commercially pure titanium [7]. However, the poor mechanical processing surface properties of Ti6Al4V implants remains today a key limitation for rapid and stable bone tissue integration. Therefore, it has become a hot and difficult issue in recent decades to find ways to reduce the surface roughness of Ti6Al4V material [5, 8].

A number of attempts have already been made to improve the surface roughness of Ti6Al4V using methods include mechanical polishing, electropolishing and pulsed laser polishing, as listed in Table 1. However, conventional mechanical polishing does not offer an acceptable solution for precision components [9, 10]. In addition, electropolishing often requires the use of strong acids and thus raises environmental and safety concerns [11]. As for laser polishing, it is not suitable in polishing optical materials [12]. Compared with the aforementioned techniques, ion beam polishing (IBP) is a noncontact, controlled and widely applicable surface polishing method

based on the well-known physical sputtering phenomenon, the erosion of atoms from a solid surface by bombardment of energetic particles [13], and can provide sample surfaces with high and reproducible quality [14]. Currently, IBP has been in active use in optical [15-19], biomedical [20, 21], geological [22-26] and other scientific research fields [27-29]. An energetic ion beam (e.g. Ar) with a relatively low energy and current density is often utilized for achieving smooth surface at microscopic length scales [30]. Beck [31] et al found that the root mean square roughness of Ni18Fe19 thin film could be reduced from to 0.45 to less than 0.3 nm by Ar^+ ion beam with the energy and current density of 70 eV and 50 μA/cm^2, respectively. Using 400 eV neon ions, the roughness of beryllium film was decreased from 1.37 down to 0.29 nm, which benefited the improvement of the reflectivity of the X-ray mirror at a wavelength of 13.5 nm[19].

Table 1 Literature status of typical Ti6Al4V polishing techniques

Polishing Techniques	Original Roughness (Ra)	Processed Roughness (Ra)	Reference
Mechanical polishing	5 μm	1.5 μm	[32]
	19.3 μm	0.3 μm	[33]
	6.4 μm	0.19 μm	[34]

	13.3 μm	5 μm	[35]
Electropolishing	4 μm	1 μm	[6]
	0.6 μm	0.3 μm	[11]
	31 μm	13 μm	[36]
Pulsed laser polishing	10.2 μm	2.4 μm	[37]
	0.206 μm	0.07 μm	[38]

Although ion beam polishing has achieved great success on obtaining of ultrasmooth surface, because of its low fluence, this method is hard to polish surfaces with a large roughness. For example, after ion beam polishing for 60 min, the roughness of polycrystalline copper was reduced only from 10.5 to 8.9 nm [26], and for larger origin roughness, it is even difficult. Therefore, in this study, mechanically finished Ti6Al4V surfaces were polished by a high current density ion beam source, and the changes of surface roughness, phase structures of the near surface layer as well as surface compositions present on typical samples were studied. Besides, the process of Ar ion bombarding the Ti6Al4V surface was also simulated by the binary collision approximation (BCA) code SDTrimSP to understand the correlations between the sputtering yield and the ion energy and ion incident angle.

2. EXPERIMENTAL

Ion beam polishing was carried out in our multi-purpose plasma immersion ion implantation facility [27], as shown in Fig. 1. An ion beam source with a diameter of 80 mm was installed on one port of the facility, the maximum current density of this ion beam source was about 3 mA/cm^2 when the ion current reached 150 mA. Φ20 × 5 mm^3 Ti6Al4V samples (nominal chemical composition in wt.%: Al-6.32, V-4.14, Fe-0.14, O-0.16, N-0.01, C-0.04, H-0.0014, and the rest is Ti) were used as substrates and the distance between the substrate and the exit of the ion source was 200 mm. Prior to the IBP, the Ti6Al4V samples received a mechanical finishing to a surface roughness, Ra, of about 0.2 μm, and were cleaned ultrasonically in acetone and alcohol bath for 10 min. Thereafter, samples were fixed on a substrate holder and inserted into the multi-purpose facility. The vacuum chamber was evacuated to a base pressure of about 4×10^{-3} Pa, then Ar (99.99%) with a mass flow rate of 50 sccm was introduced into the vacuum chamber, the working pressure during the IBP process was kept at 2×10^{-2} Pa. The ion current, energy and incident angle between the ion beam and the sample surfaces were systematically varied according to the detailed parameters listed in Table 2. In addition, in order to compare the roughness change during the ion beam polishing process for each sample, one half of the processing surface was masked by a 0.02 mm thick aluminum foil. Meanwhile, a k-type thermocouple was connected to the sample and the temperatures in the ion beam polishing process were recorded.

Table 2 Ion beam polishing parameters for the Ti6Al4V samples

Sample No.	Ion current (mA)	Ion energy (eV)	Incident angle (°)
S11	85	600	75
S12	100	600	75
S13	115	600	75
S14	130	600	75
S15	145	600	75
S21	130	300	75
S22	130	400	75
S23	130	500	75
S24	130	700	75
S31	130	600	65
S32	130	600	70
S33	130	600	80
S34	130	600	85

Surfaces of the ion beam polished samples were imaged by laser scanning confocal microscopy (LSCM; Olympus, OLS3000, Japan) with a scanning area of 256×256 μm^2, and the surface roughness was calculated according to the LSCM result. In order to obtain an accurate roughness, nine regions of 8.1 × 8.1 μm^2 were examined

for each sample, and the mean value was taken. Surface topology of the original as well as polished Ti6Al4V samples was also measured by atomic force microscope (AFM; Dimension Icon, Bruker Corporation, Germany). The phase transition of the samples before and after ion beam polishing were identified by grazing incidence X-ray diffraction (GIXRD; Bruker, D8 ADVANCE, Germany) at an incident angle of 1° with Cu Kα (λ=0.15418 nm) radiation operated at 40 kV and 40 mA. The elemental composition of the sample surfaces were examined by X-ray photoelectron spectrometer (XPS; Thermo Fisher Scientific, ESCALAB 250Xi, USA).

3. RESULTS AND DISCUSSION

3.1 Experimental

Fig. 2 shows the temperature evolution during the IBP process under different ion currents and energies (samples S11-S15 and S21-S24). It can be found that the temperature increased rapidly in the first 20 minutes and then rose slowly in the following period. The highest temperature reached was about 200 ℃ when the current and energy of the ion beam were 145 mA and 700 eV, respectively. As we know, the heat generated by ion bombardment was proportional to the power density and the impinging time of the ion beam, consequently, the temperature evolution process was decided by both parameters. Besides, although a large current density ion source was used in our experiments, it is clear that the maximum temperature should not too high

for the Ti6Al4V substrate.

The LSCM images of the samples under different ion beam currents are shown in Fig. 3. The left half of each figure indicates the surface after the IBP process, while the right half is the surface without the ion beam treatment. It is clear that a high density of pits, which should be derived from the mechanical polishing process, located in the right half of each image. However, after the IBP treatment, as shown in the left half of all images, the density of pits in all samples decreased greatly. In addition, the density of pits was also varied with the ion beam parameters, the sample under an ion beam current of 130 mA had the fewest quantities of pits. Therefore, the LSCM images proved that the surface roughness of the samples could be reduced after the ion beam polishing process.

According to the LSCM images, we also obtained the surface roughness of all samples. Fig. 4(a) compares the roughness change of samples under different ion beam currents (samples S11-S15). It can be found that the original roughness (OR) of all samples was about 0.2 μm. After the IBP treatment, the processing roughness (PR) was decreased to about 1/3 of the original value. Meanwhile, the inter-quartile ranges (IQR) were reduced greatly. In addition, it is also obvious that if the IQR of the original sample was small, the inter-quartile range of the polished one was small too. To give a more explicit picture of the influence of the ion current, the surface roughness of samples after the ion beam polishing process was plotted in Fig. 4(b), it is clear that the mean roughness of all samples decreased with the increasing ion

current. Therefore, in order to obtain a good smoothing effect, we should use a relative large ion beam current.

Fig. 5 shows the relationship between the ion energy and the surface roughness (samples S14, S21-S24). As can be seen that the roughness of the all samples decreased greatly, and sample polished with an ion energy of 600 eV, possess the smallest roughness. However, when the incident ion energy was too small (300 eV), both the surface roughness and IQR increased greatly. Hence, the optimum energy range for ion beam polishing of the Ti6Al4V sample should be between 400 and 700 eV. Since there have been some researches with good surface roughness improvement results of a variety of metal materials by low energy IBP [39, 40], together with the experiment results, the Ar ion energy to proceed the following research is chosen to be 600 eV.

Fig. 6 shows the influence of the ion incident angle on the surface roughness (samples S14, S31-S34). It is evident that the mean surface roughness was decreased to a value below 60 nm, which hints that a good surface smoothing effect was obtained for all samples. In addition, the sample using an impact angle of 75 °had the lowest mean roughness of about 53 nm, a change of the incident angle to 65 °and 85 ° raised the mean surface roughness by about 10 and 15 %, respectively.

The sputtering effect on roughness evolution involves a complex mechanism, which has both smoothing and roughening effects. The passivation effect of IBP on micro-particles and scratches makes the surface smoother. However, IBP will also

remove the abrasives and impurities embedded in the subsurface layer and thus form many pits on the surface, resulting in the deterioration of roughness. In addition, the uneven distribution of surface stress introduced during the traditional surface treatment processes such as lapping and polishing lead to the inconsistency of the sputtering removal rate, which also makes the roughness worse. The final roughness evolution depends on the dynamic equilibrium of the smoothing effect and the roughing effect [41]. In summary, the IBP process is very sensitive to the originally existing surface/subsurface damages, like scratches and residual impurities. For the anisotropy of the microscopic material, the morphology evolution process would be seriously influenced by the difference of the sputtering rate, which finally limits the smoothing effect of Ti6Al4V [41, 42]. Similar results have been reported with the result that initially smoother substrates exhibit a lower surface roughness after ion erosion related to initially rougher substrates [43-47].

The AFM topology measurements were performed at both $1 \times 1 \mu m^2$ and 10×10 μm^2 scan sizes. A conventional Si tips with a tip radius of 10 nm was used to ensure the accuracy of the AFM results and to minimize any tip convolution of the shape measured. The AFM images for the original mechanically finished Ti6Al4V and sample polished with an ion incidence angle of $75°$ and ion energy of 600 eV (S14) are shown in Fig. 7. The comparison of the 10×10 μm^2 AFM images indicates that there is a significant smoothing of the roughness on the Ti6Al4V surface.

To investigate the smoothing effect of this technique in detail, we calculated the

power spectral density (PSD) functions from the scan line profile measurement of the AFM data, as shown in Fig. 8. For each sample, the PSD functions computed at two scan sizes were combined in a single PSD curve with an extended range of spatial frequencies. The results indicate that processing by argon ions allows effective smoothing the surface of Ti6Al4V over all spatial frequencies included by the AFM measurements. Moreover, it can also be recognized that the degree of surface smoothing is different depending on the spatial frequency of the surface roughness, which tends to degrade with decreasing spatial frequency.

In order to determine the influence of the ion beam polishing parameters on the phase structures of the surface layer, we compared the grazing incidence X-ray diffraction patterns (GIXRD) of the samples before and after the ion beam smoothing process in Fig. 9. The obvious strong peaks at about 35.5 °, 38.9 °, 40.6 °, and 78.6 ° in the patterns confirmed that the Ti6Al4V samples mainly contain the hexagonal close packed (HCP) α-Ti, our lab-based GIXRD facility was not able to recognize the peaks of the body centered cubic (BCC) β-Ti [48-50]. Furthermore, it is quite obvious that the intensities and positions of the diffraction peaks for all samples were similar. The GIXRD results are also consistent with those obtained in Fig.2, the highest temperature reached in this experiment was about 200 ℃, which is not enough to trigger any phase transition in the samples. Therefore, the influence of ion beam polishing process on the phases of the sample can be neglected.

Fig. 10 compares the XPS survey spectra of the original and sample polished

with 600 eV ion energy and 75 ° incident angle (S14). During these measurements the original sample was etched inside the XPS chamber by 2 keV Ar ion gun to obtain the true elemental composition of pure Ti6Al4V surface, while the ion beam polished samples did not. It can be easily confirmed that elements C, O, Ti, Al and V are present in all the samples, in addition, a higher signal for oxygen can also be observed in the ion beam polished sample. This is likely to be due to the fact that Ti, Al and V are highly reactive metal, so when the alloying elements are exposed to the atmosphere, it is easily for them to form natural passive layers of corresponding oxides.

To investigate the chemical composition in detail and determine the surface oxidation states of samples polished by different ion incident angles, high resolution scans of Ti 2p, Al 2p and V 2p spectra are shown in Fig. 11. The spectrum obtained for Ti, Al and V in the original sample shows that the presence of the three alloying elements is in its metallic form. However, as for the ion beam polished samples, a characteristic doublet peak with the binding energy of 458.1 ± 0.2 and 463.8 ± 0.2 eV appears for all the polished samples, showed that Ti is mainly present on the surface as Ti^{3+} [51]. Furthermore, both the Al and V elements are composed of single weak peak, which located at 74.2 ± 0.2 (Al^{3+}) and 516.9 ± 0.2 (V^{5+}), respectively. Hence, it is evident that the surface of all the polished samples were dominated by Ti_2O_3 and Al_2O_3, with small quantities of V_2O_5 exist as interstitial or substitutional in the Ti_2O_3 matrix [52].

Fig. 12 compares the atomic concentrations of the main components of Ti6Al4V on surface of original and ion beam polished samples. Compared with the original Ti6Al4V sample, the concentration of Ti decreased significantly in all the polished samples, but it did not change much for samples polished by different ion incident angles. While for Al element, the change of its concentration after the IBP process is opposite from that of the Ti. However, noticeable variations in the concentration of the much lower V element present on the surface of control samples were not detected. We also need to realize that although the XPS results confirmed that oxide film were formed on the surface of the ion beam polished Ti6Al4V samples, the self-formed oxide films (Ti_2O_3, Al_2O_3 and V_2O_5) were too thin to be detected by the GIXRD technique, so only the diffraction peaks belong to HCP α-Ti were identified in Fig. 9 [53, 54].

3.2 Modelling with SDTrimSP

Since the IBP is a complicated process with the production of sputtering, backscattered as well as implanted ions within the target material. Theoretical calculation, by using SDTrimSP code, is also performed to analyze the dependence of the sputtering yield on ion incidence angle and ion energy. SDTrimSP, similar to the widely used TRIM, is a binary collision approximation (BCA) code that simulates the interaction of energetic particles (e.g. Ar) with a target (e.g. Ti6Al4V) and allows dynamical changes within the target (the incorporation of projectile atoms, atomic mixing as well as preferential sputtering) [55-58]. In addition, it does not have the

drawbacks that existed in TRIM, such as wrong angular distribution of sputtered atoms for targets containing low atomic number (Z) elements with Z < 14 and overestimation of the high angle sputtering yield[59]. The SDTrimSP calculations were performed with the input parameters similar to the program described in [15] with Ar ion energy from 300 eV to 1000 eV, and ion incident angle in the range of 0 ° to 85 °[60]. Using this model, the energy and angular dependence of the sputtering yield were investigated [61].

Calculated correlation between sputtering yield and ion energy at the fixed incident angle of 75 ° is given in Fig. 13. As can be seen that the sputtering yield of target atoms (Ti, Al and V) increases almost linearly with the increasing ion energy. When the ion energy is 300 eV, the sputtering coefficient of Ti is relatively low, about 0.6, which should be the main reason for the high surface roughness of the sample S21 shown in Fig. 5. In addition, it can also be found that the sputtering yield of Ti is the largest, as Ti is the most abundant element in this Ti6Al4V material. Fig. 14 shows the sputtering yield of Ti6Al4V at different ion incident angles when the ion energy fixed at 600 eV. The calculated results look very similar to those observed for other materials [62]. As can be seen, the sputtering yield first increases gradually with increasing incident angle, starting at about 0.7-Ti, 0.08-Al and 0.03-V atoms/ion for normal incidence (0 °) and peak at about 2.0-Ti, 0.23-Al and 0.09-V atoms/ion at an incidence angle of about 65 °. However, it decreased rapidly at higher angles (larger than 70 °) because the incident direction is almost parallel to the sample surface,

which will leads to more reflection of the bombard Ar ions.

4. CONCLUSIONS

Ti6Al4V samples with a surface roughness of about 0.2 μm were successfully polished by ion beams with a high current density. The lowest mean roughness reached is a bioactive nanotextured Ti6Al4V surface of 53 nm with an ion energy, current and incident angle of 600 eV, 130 mA and 75 °, respectively. Furthermore, as confirmed by the GIXRD results, the phase structures of the Ti6Al4V samples kept steady after the IBP process. The XPS results revealed that C, O, Ti, Al and V are present in both the original as well as the polished samples. In addition, a higher signal for oxygen can also be found on the surface of the ion beam polished samples. Theoretical calculations, by the use of SDTrimSP code, have also been presented to investigate the relationship between the sputtering yield and ion beam parameters. The results confirmed that best smoothing effect comes from the sample which has a medium sputtering yield.

ACKNOWLEDGMENT

This work was financially supported by the fund of National Key Research and Development Program of China (2017YFC0111002).

REFERENCES

[1] X. Liu, P. Chu, C. Ding, Surface modification of titanium, titanium alloys, and related materials for biomedical applications, Mat. Sci. Eng. R 47 (2004) 49-121.

[2] M. Navarro, A. Michiardi, O. Castano, J.A. Planell, Biomaterials in orthopaedics, J. R. Soc. Interface 5 (2008) 1137-1158.

[3] M. Geetha, A.K. Singh, R. Asokamani, A.K. Gogia, Ti based biomaterials, the ultimate choice for orthopaedic implants – A review, Prog. Mater. Sci. 54 (2009) 397-425.

[4] Q. Chen, G.A. Thouas, Metallic implant biomaterials, Mat. Sci. Eng. R 87 (2015) 1-57.

[5] L. Salou, A. Hoornaert, G. Louarn, P. Layrolle, Enhanced osseointegration of titanium implants with nanostructured surfaces: an experimental study in rabbits, Acta Biomater. 11 (2015) 494-502.

[6] V. Urlea, V. Brailovski, Electropolishing and electropolishing-related allowances for powder bed selectively laser-melted Ti-6Al-4V alloy components, J. Mater. Process Tech. 242 (2017) 1-11.

[7] C. Boehlert, M. Niinomi, M. Ikeda, Introduction, Mat. Sci. Eng. C-Mater. 25 (2005) 247.

[8] A.S. Guilherme, G.E. Henriques, R.A. Zavanelli, M.F. Mesquita, Surface roughness and fatigue performance of commercially pure titanium and Ti-6Al-4V alloy after different polishing protocols, J. Prosthet. Dent. 93 (2005) 378-385.

[9] M.-Y. Tsai, W.-Z. Yang, Combined ultrasonic vibration and chemical mechanical polishing of copper substrates, Int. J. Mach. Tool. Manu. 53 (2012) 69-76.

[10] Y. Li, Y. Wu, L. Zhou, M. Fujimoto, Vibration-assisted dry polishing of fused silica using a fixed-abrasive polisher, Int. J. Mach. Tool. Manu. 77 (2014) 93-102.

[11] M.A. Birch, S. Johnson-Lynn, S. Nouraei, Q.B. Wu, S. Ngalim, W.J. Lu, C. Watchorn, T.Y. Yang, A.W. McCaskie, S. Roy, Effect of electrochemical structuring of Ti6Al4V on osteoblast behaviour in vitro, Biomed. Mater. 7 (2012) 035016.

[12] R.M. Wood, Laser-induced damage of optical materials, CRC Press, 2003.

[13] P. Sigmund, Recollections of fifty years with sputtering, Thin Solid Films 520 (2012) 6031-6049.

[14] G. Carter, The physics and applications of ion beam erosion, J. Phys. D. Appl. Phys. 34 (2001) R1-R22.

[15] W. Liao, Y. Dai, X. Xie, L. Zhou, Morphology evolution of fused silica surface during ion beam figuring of high-slope optical components, Appl. Optics 52 (2013) 3719-3725.

[16] H.A. MacEwen, J.F. Ellison, G.P. Cox, L.J. Sutton, A.C. Fox, T.M. Rich, T.A. Sebring, J.B. Breckinridge, Benefits of ion milling ULE as compared to glass ceramics, SPIE Proc. 8860(2013):88600O

[17] N.I. Chkhalo, S.A. Churin, A.E. Pestov, N.N. Salashchenko, Y.A. Vainer, M.V. Zorina, Roughness measurement and ion-beam polishing of super-smooth optical surfaces of fused quartz and optical ceramics, Opt. Express 22 (2014) 20094-20106.

[18] N.I. Chkhalo, I.A. Kaskov, I.V. Malyshev, M.S. Mikhaylenko, A.E. Pestov, V.N. Polkovnikov, N.N. Salashchenko, M.N. Toropov, I.G. Zabrodin, High-performance facility and techniques for high-precision machining of optical components by ion beams, Precis. Eng. 48 (2017) 338-346.

[19] N.I. Chkhalo, M.S. Mikhailenko, A.V. Mil'kov, A.E. Pestov, V.N. Polkovnikov, N.N. Salashchenko, I.L. Strulya, M.V. Zorina, S.Y. Zuev, Effect of ion beam etching on the surface

roughness of bare and silicon covered beryllium films, Surf. Coat. Tech. 311 (2017) 351-356.
[20] L.A. Giannuzzi, D. Phifer, N.J. Giannuzzi, M.J. Capuano, Two-dimensional and 3-dimensional analysis of bone/dental implant interfaces with the use of focused ion beam and electron microscopy, J. Oral. Maxillofac. Surg. 65 (2007) 737-747.
[21] D. Grüner, J. Fäldt, K. Jansson, Z. Shen, Argon ion beam polishing: a preparation technique for evaluating the interface of osseointegrated implants with high resolution, Int. J. Oral. Maxillofac. Implants. 26 (2011) 547-552.
[22] R.G. Loucks, R.M. Reed, S.C. Ruppel, U. Hammes, Spectrum of pore types and networks in mudrocks and a descriptive classification for matrix-related mudrock pores, AAPG Bull. 96 (2012) 1071-1098.
[23] S. Giffin, R. Littke, J. Klaver, J.L. Urai, Application of BIB–SEM technology to characterize macropore morphology in coal, Int. J. Coal. Geol. 114 (2013) 85-95.
[24] M.E. Houben, G. Desbois, J.L. Urai, Pore morphology and distribution in the Shaly facies of Opalinus Clay (Mont Terri, Switzerland): Insights from representative 2D BIB–SEM investigations on mm to nm scale, Appl. Clay. Sci. 71 (2013) 82-97.
[25] R.G. Loucks, R.M. Reed, Scanning-electron-microscope petrographic evidence for distinguishing organic matter pores associated with depositional organic matter versus migrated organic matter in mudrocks, Gcags Trans. 3 (2014) 51-60.
[26] A. Grobe, J. Schmatz, R. Littke, J. Klaver, J.L. Urai, Enhanced surface flatness of vitrinite particles by broad ion beam polishing and implications for reflectance measurements, Int. J. Coal. Geol. 180 (2017) 113-121.
[27] O. Wada, Ar ion-beam etching characteristics and damage production in InP, J. Phys. D Appl. Phys. 17 (1984) 2429-2437.
[28] E.J. Knystautas, D.B. Fenner, V. DiFilippo, J. Bennett, T. Tetreault, J.K. Hirvonen, L.C. Feldman, W.P. Kirk, V. Browning, Ion beam nanosmoothing of sapphire and silicon carbide surfaces, Proc. SPIE - Int. Soc. Opt. Eng. 4468 (2001) 17-24.
[29] A. Schindler, Ion beam milling of optically polished CaF2 surfaces, in: Optical Manufacturing and Testing V, 2003, pp. 81-88.
[30] A. Mutzke, A. Rai, R. Schneider, E.J. Angelin, R. Hippler, Modeling of altered layer formation during reactive ion etching of GaAs, Appl. Surf. Sci. 263 (2012) 626-632.
[31] P.A. Beck, B.F.P. Roos, S.O. Demokritov, B. Hillebrands, Ion beam smoothing with low-energy argon ions and reduction of Néel “orange peel” coupling in magnetic tunnel junctions, J. Magn. Magn. Mater. 290-291 (2005) 1108-1111.
[32] C.H. Che-Haron, A. Jawaid, The effect of machining on surface integrity of titanium alloy Ti–6% Al–4% V, J. Mater. Process. Techn. 166 (2005) 188-192.
[33] S. Bagehorn, T. Mertens, D. Greitemeier, L. Carton, A. Schoberth, Surface finishing of additive manufactured Ti-6Al-4V - a comparison of electrochemical and mechanical treatments, 6th Eur. Conf. Aerosp. Sci. (2015).
[34] A. Boschetto, L. Bottini, F. Veniali, Surface roughness and radiusing of Ti6Al4V selective laser melting-manufactured parts conditioned by barrel finishing, Int. J. Adv. Manu. Tech. 94 (2017) 2773-2790.
[35] A.F. Teixeira, Development of an Electropolishing Method for Titanium Materials, Thesis

Dissertention, Concordia University, 2013.
[36] A. Mohammad, M.K. Mohammed, A.M. Alahmari, Effect of laser ablation parameters on surface improvement of electron beam melted parts, Int. J. Adv. Manu. Tech. 87 (2016) 1033-1044.
[37] S. Marimuthu, A. Triantaphyllou, M. Antar, D. Wimpenny, H. Morton, M. Beard, Laser polishing of selective laser melted components, Int. J. Mach. Tool. Manu. 95 (2015) 97-104.
[38] T.L. Perry, D. Werschmoeller, X. Li, F.E. Pfefferkorn, N.A. Duffie, Pulsed laser polishing of micro-milled Ti6Al4V samples, J. Manuf. Process. 11 (2009) 74-81.
[39] N.I. Chkhalo, E.B. Kluenkov, A.E. Pestov, V.N. Polkovnikov, D.G. Raskin, N.N. Salashchenko, L.A. Suslov, M.N. Toropov, Manufacturing of XEUV mirrors with a sub-nanometer surface shape accuracy, Nucl. Instru. Meth. A 603 (2009) 62-65.
[40] M.M. Barysheva, Y.A. Vainer, B.A. Gribkov, M.V. Zorina, A.E. Pestov, N.N. Salashchenko, R.A. Khramkov, N.I. Chkhalo, The evolution of roughness of supersmooth surfaces by ion-beam etching, Bull. Russ. Acad. Sci. 76 (2012) 163-167.
[41] M. Xu, Y. Dai, L. Zhou, X. Peng, S. Chen, W. Liao, Evolution mechanism of surface roughness during ion beam sputtering of fused silica, Appl. Optics 57 (2018) 5566-5573.
[42] W. Liao, X. Nie, Z. Liu, X. Nie, W. Wan, Researches on formation mechanism of ultra-smooth surface during ion beam sputtering of fused silica, Optik 179 (2019) 957-964.
[43] P. Mishra, D. Ghose, Formation of nanoripples in Al films duringO2+sputtering, Phys. Rev. B 74 (2006).
[44] P. Karmakar, S.A. Mollick, D. Ghose, A. Chakrabarti, Role of initial surface roughness on ion induced surface morphology, Appl. Phys. Lett. 93 (2008) 103102.
[45] S. Sarkar, B.V. Daele, W. Vandervorst, Impact of repetitive and random surface morphologies on the ripple formation on ion bombarded SiGe-surfaces, New J. Phys. 10 (2008) 083012.
[46] A. Toma, B.Š. Batič, D. Chiappe, C. Boragno, U. Valbusa, M. Godec, M. Jenko, F. Buatier de Mongeot, Patterning polycrystalline thin films by defocused ion beam: The influence of initial morphology on the evolution of self-organized nanostructures, J. Appl. Phys. 104 (2008) 104313.
[47] J.H. Kim, M. Joe, S.P. Kim, N.B. Ha, K.R. Lee, B. Kahng, J.S. Kim, Pattern evolution on previously rippled Au(001) by crossing-ion-beam sputtering, Phys. Rev. B 79 (2009).
[48] H. Yu, M. Yan, C. Lu, A.K. Tieu, H. Li, Q. Zhu, A. Godbole, J. Li, L. Su, C. Kong, Superstrength of nanograined steel with nanoscale intermetallic precipitates transformed from shock-compressed martensitic steel, Sci. Rep. 6 (2016) 36810.
[49] J.Y. Lek, A. Bhowmik, A.W.-Y. Tan, W. Sun, X. Song, W. Zhai, P.J. Buenconsejo, F. Li, E. Liu, Y.M. Lam, C.B. Boothroyd, Understanding the microstructural evolution of cold sprayed Ti-6Al-4V coatings on Ti-6Al-4V substrates, Appl. Surf. Sci. 459 (2018) 492-504.
[50] H. Zhou, C. Li, G. Ji, S. Fu, H. Yang, X. Luo, G. Yang, C. Li, Local microstructure inhomogeneity and gas temperature effect in in-situ shot-peening assisted cold-sprayed Ti-6Al-4V coating, J. Alloy. Compd. 766 (2018) 694-704.
[51] M. Ask, J. Lausmaa, B. Kasemo, Preparation and surface spectroscopic characterization of oxide films on Ti6Al4V, Appl. Surf. Sci. 35 (1989) 283-301.
[52] F. Variola, J.H. Yi, L. Richert, J.D. Wuest, F. Rosei, A. Nanci, Tailoring the surface properties of Ti6Al4V by controlled chemical oxidation, Biomaterials 29 (2008) 1285-1298.
[53] H. Güleryüz, E. Atar, F. Seahjani, H. Çimenoğlu, An Overview on Surface Hardening of

Titanium Alloys by Diffusion of Interstitial Atoms, Diff. Found. 4 (2015) 103-116.
[54] M.S. El-Eskandrany, A. Al-Azmi, Potential applications of cold sprayed Cu50Ti20Ni30 metallic glassy alloy powders for antibacterial protective coating in medical and food sectors, J. Mech. Behav. Biomed. Mater. 56 (2016) 183-194.
[55] W. Möller, W. Eckstein, Tridyn — A TRIM simulation code including dynamic composition changes, Nucl. Instru. Meth. B 2 (1984) 814-818.
[56] H. Hofsäss, K. Zhang, A. Mutzke, Simulation of ion beam sputtering with SDTrimSP, TRIDYN and SRIM, Appl. Surf. Sci. 310 (2014) 134-141.
[57] D.P. Datta, S.K. Garg, T. Basu, B. Satpati, H. Hofsäss, D. Kanjilal, T. Som, Temporal evolution of Ge surface topography under keV ion irradiation: Combined effects of curvature-dependent sputter erosion and atomic redistribution, Appl. Surf. Sci. 360 (2016) 131-142.
[58] V.I. Shulga, Angle-dependent sputter yield of rippled surfaces, Appl. Surf. Sci. 458 (2018) 18-23.
[59] A. Mutzke, W. Eckstein, Ion fluence dependence of the Si sputtering yield by noble gas ion bombardment, Nucl. Instru. Meth. B 266 (2008) 872-876.
[60] P.S. Szabo, R. Chiba, H. Biber, R. Stadlmayr, B.M. Berger, D. Mayer, A. Mutzke, M. Doppler, M. Sauer, J. Appenroth, J. Fleig, A. Foelske-Schmitz, H. Hutter, K. Mezger, H. Lammer, A. Galli, P. Wurz, F. Aumayr, Solar wind sputtering of wollastonite as a lunar analogue material – Comparisons between experiments and simulations, Icarus 314 (2018) 98-105.
[61] R. Stadlmayr, P.S. Szabo, B.M. Berger, C. Cupak, R. Chiba, D. Blöch, D. Mayer, B. Stechauner, M. Sauer, A. Foelske-Schmitz, M. Oberkofler, T. Schwarz-Selinger, A. Mutzke, F. Aumayr, Fluence dependent changes of surface morphology and sputtering yield of iron: Comparison of experiments with SDTrimSP-2D, Nucl. Instru. Meth. B 430 (2018) 42-46.
[62] R. Behrisch, W. Eckstein, Sputtering by Particle Bombardment: Experiments and Computer Calculations from Theshold to MeV energies, Springer, 2007.

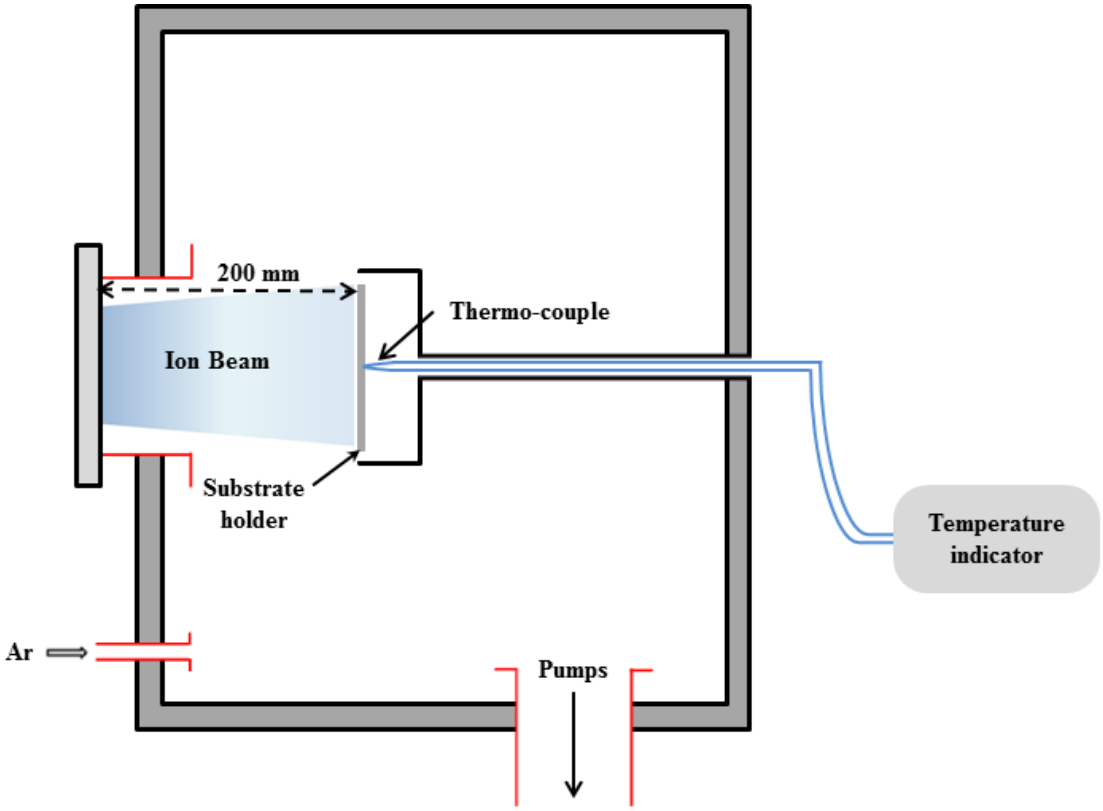

Fig. 1 Schematic diagram of the experimental setup

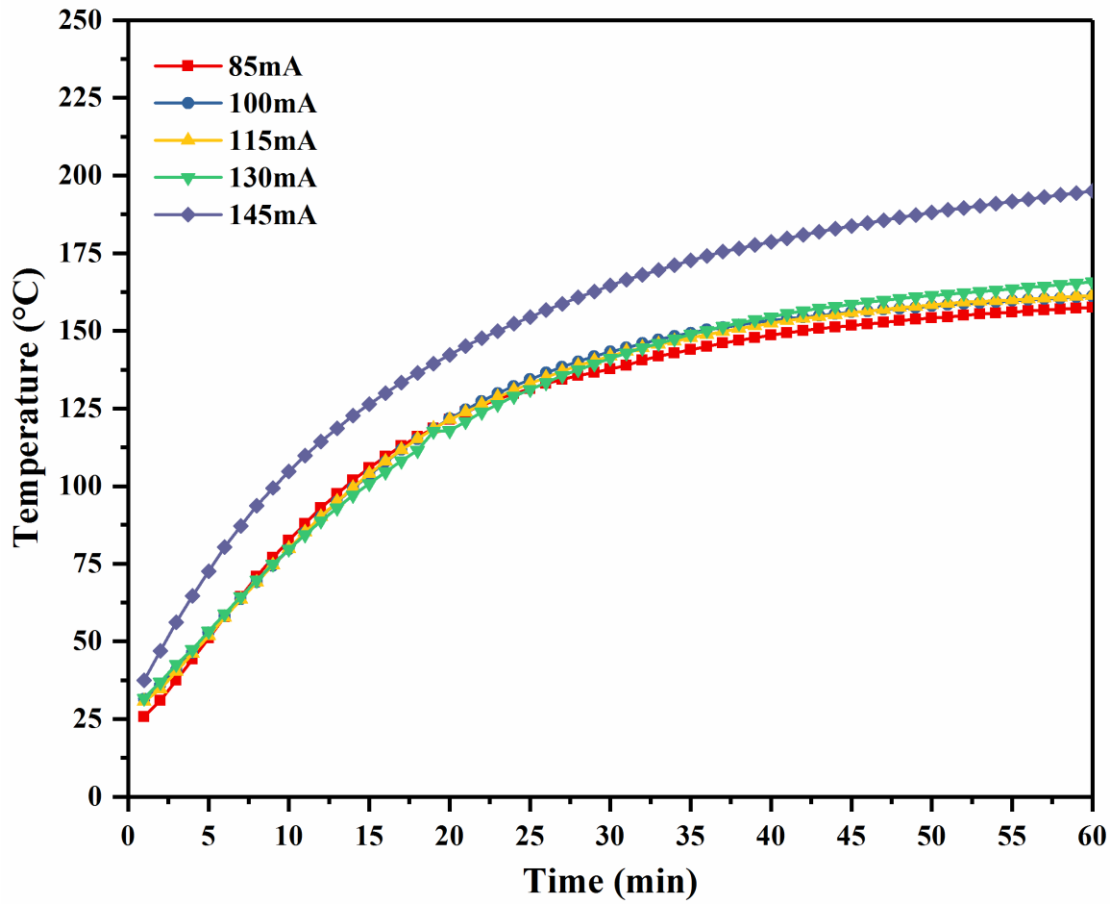
85mA
100mA
115mA
130mA
145mA
Temperature (°C)
Time (min)
0
25
50
75
100
125
150
175
200
225
250
0
5
10
15
20
25
30
35
40
45
50
55
60

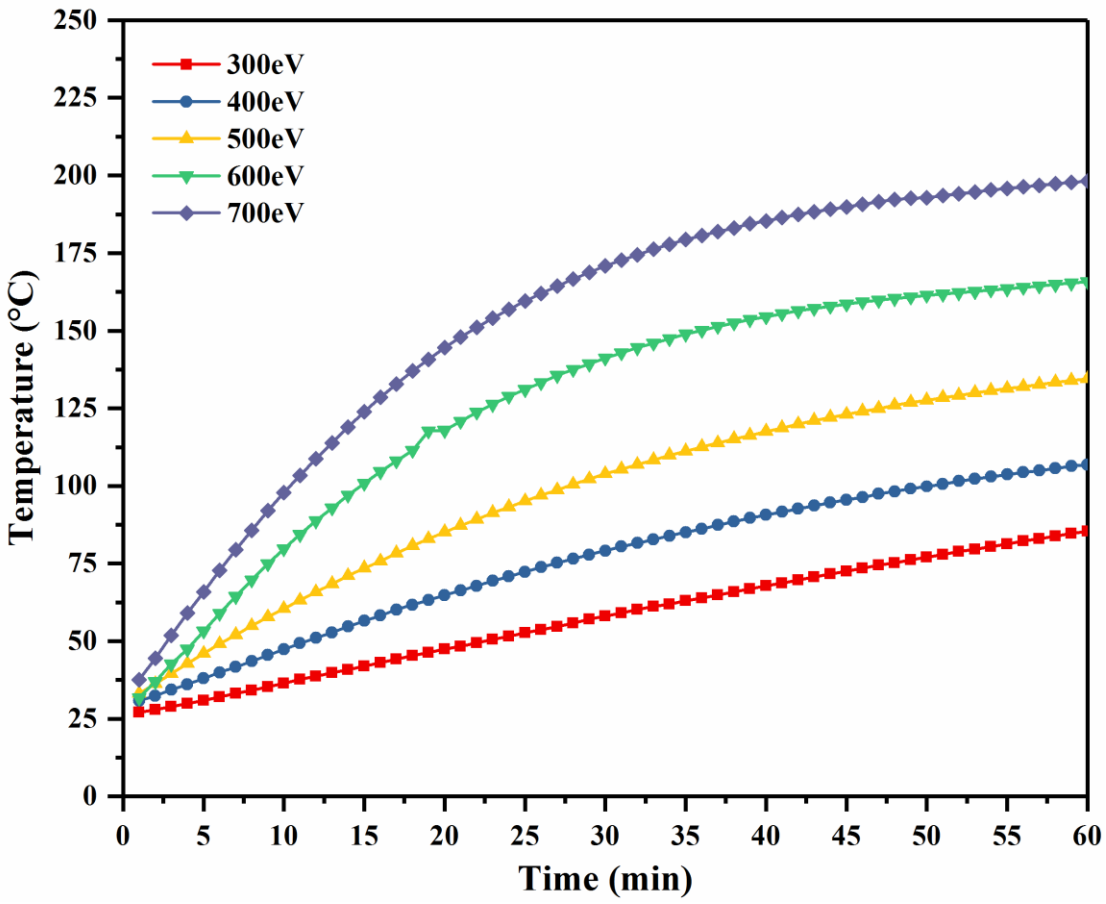

Fig. 2 Temperature evolution during the ion beam polishing process under different ion beam currents (a) and energies (b)

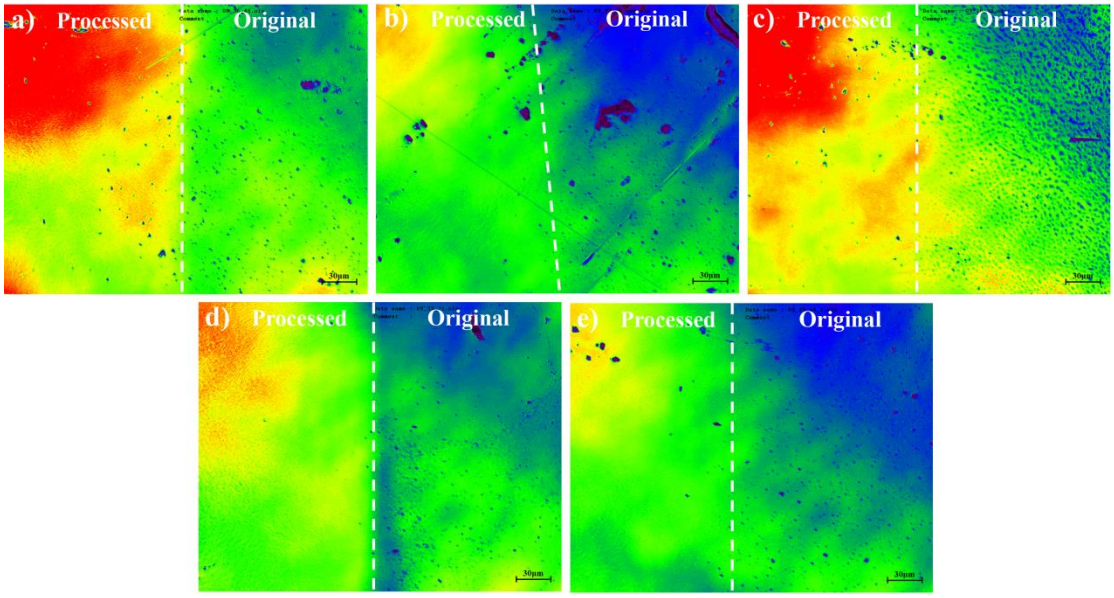

Fig. 3 LSCM images of samples polished under different ion currents. (a) 85mA, (b) 100mA, (c) 115mA, (d) 130mA, (e) 145mA

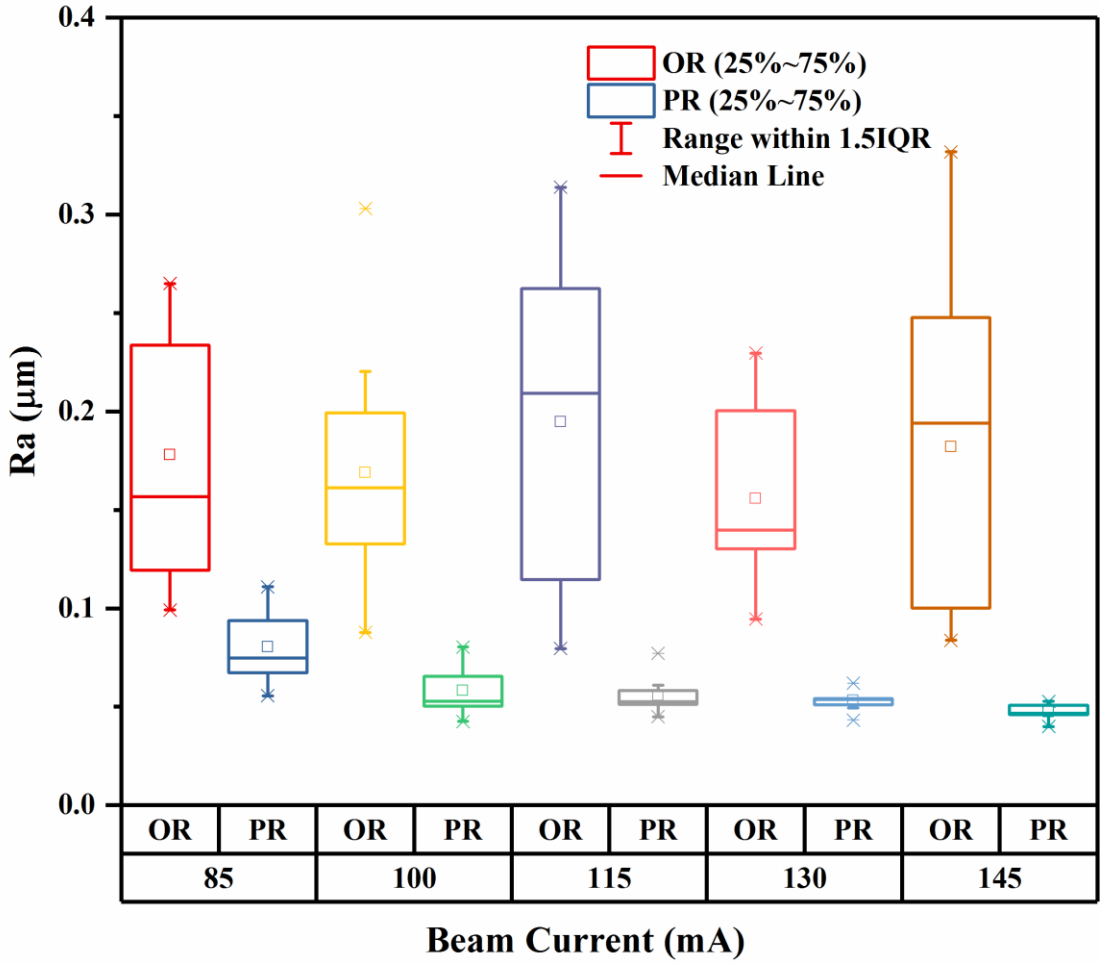
OR (25%~75%)
PR (25%~75%)
Range within 1.5IQR
Median Line
Ra (μm)
0.0
0.1
0.2
0.3
0.4
OR
PR
OR
PR
OR
PR
OR
PR
OR
PR
85
100
115
130
145
Beam Current (mA)

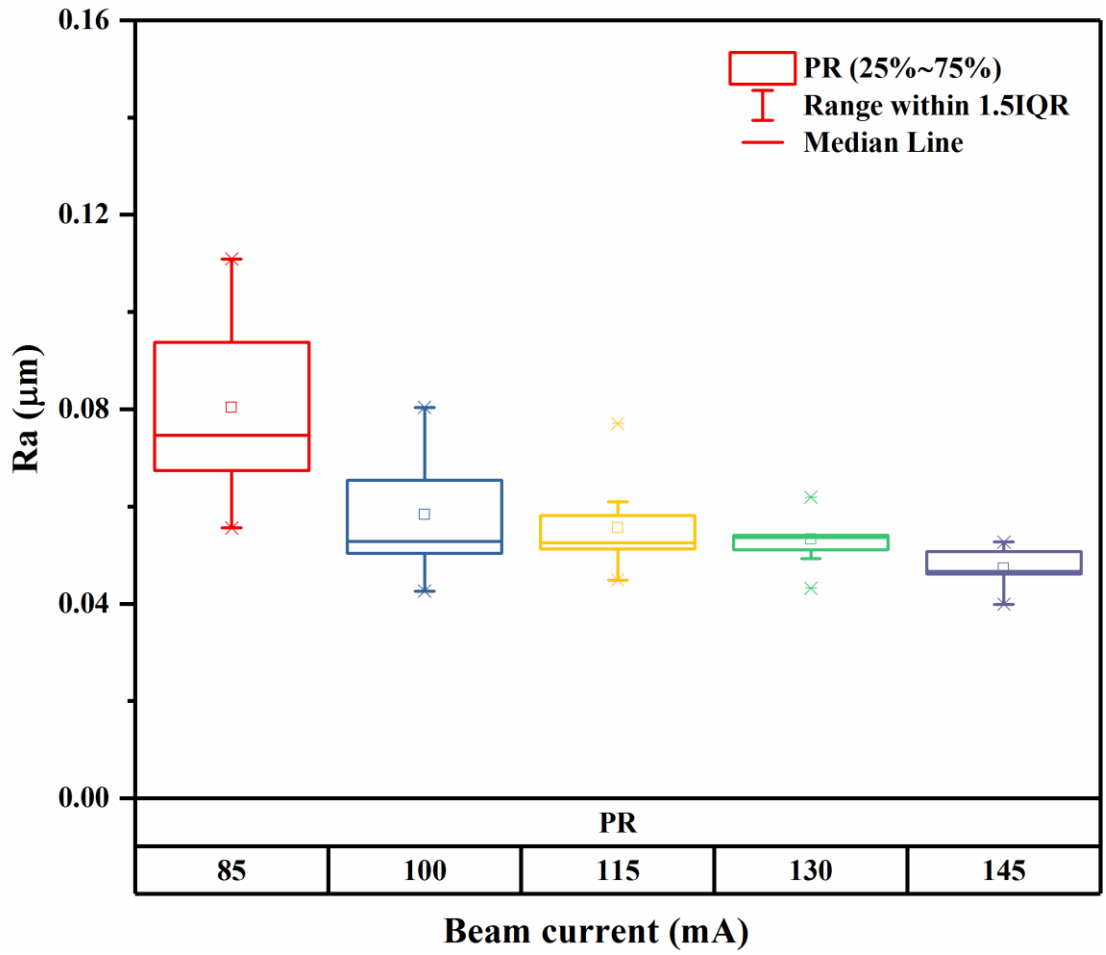

Fig. 4 Surface roughness of the original and polished samples (a) and the influence of ion current on the surface roughness of polished samples (b).

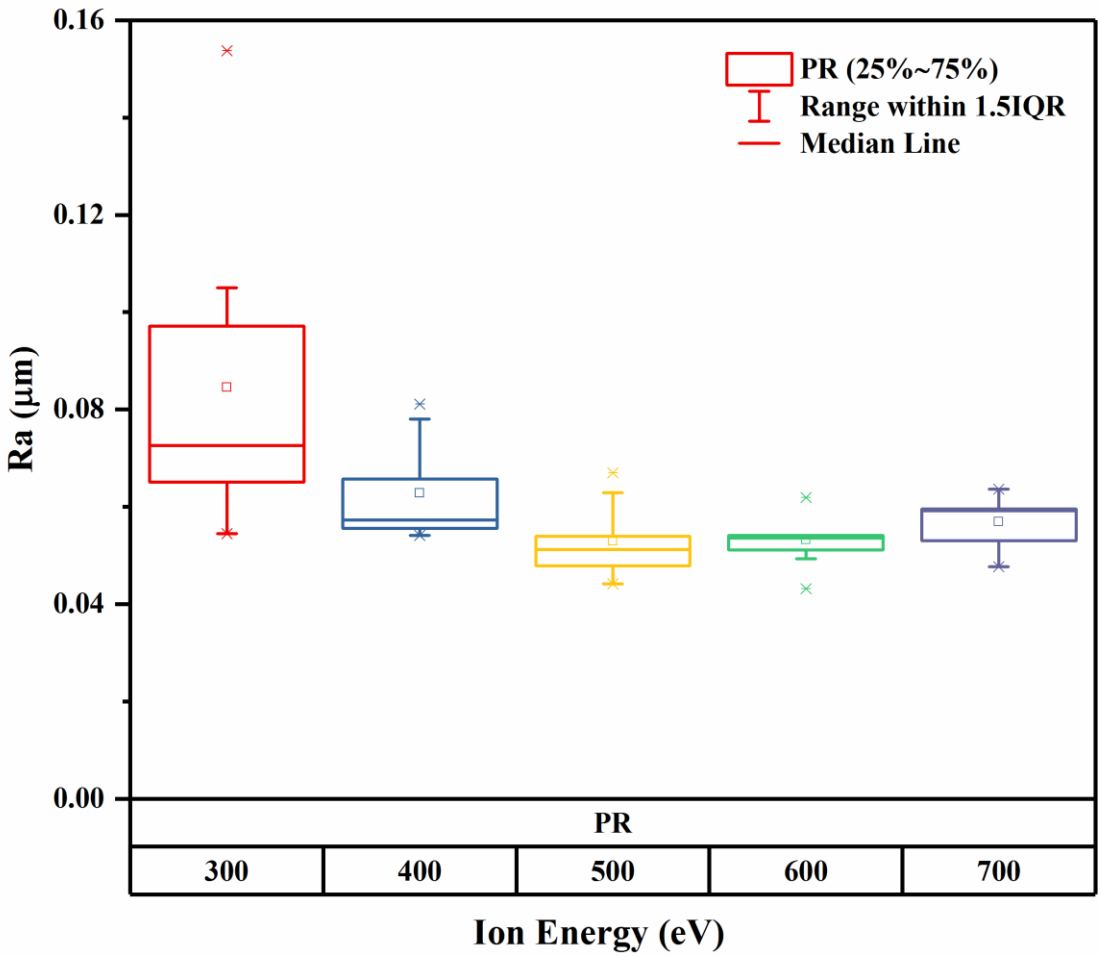

Fig. 5 Relationship between the incident ion energy and the surface roughness.

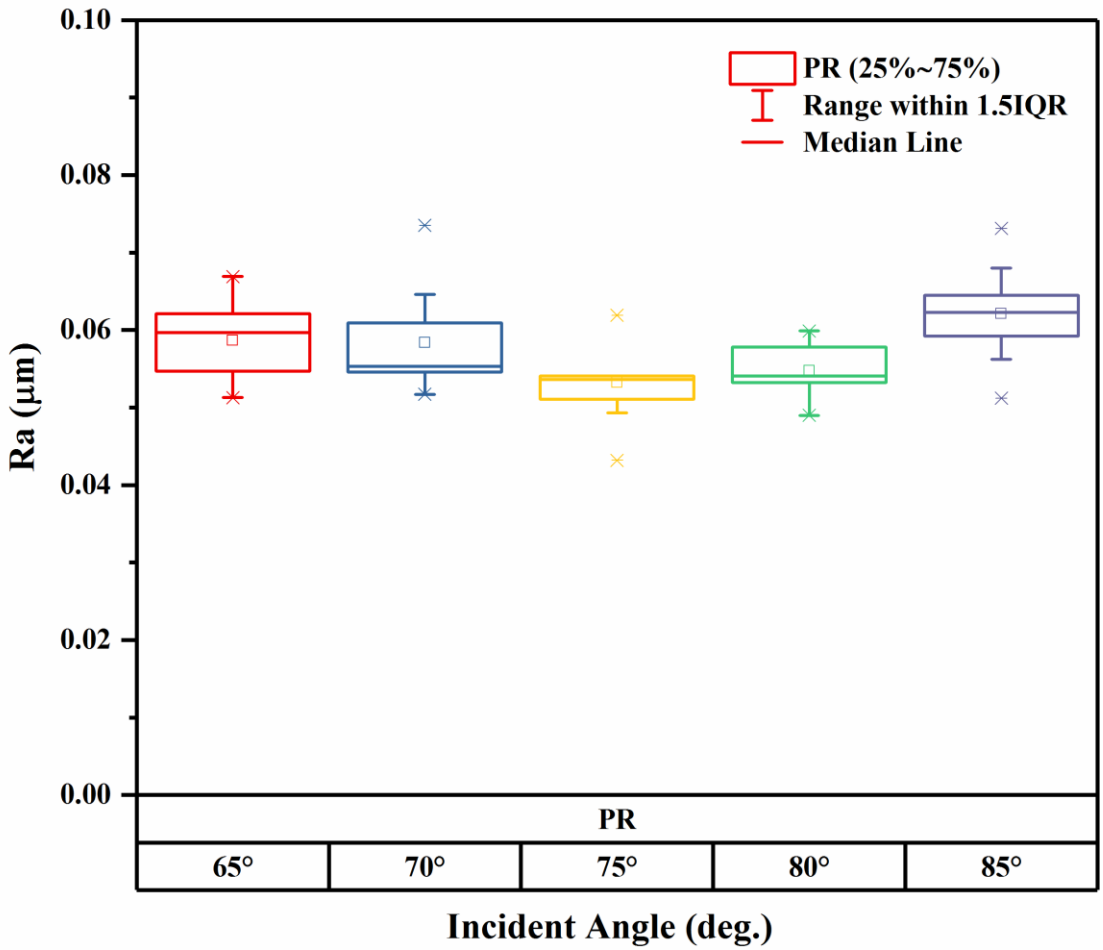

Fig. 6 Relationship between the ion incident angle and the surface roughness

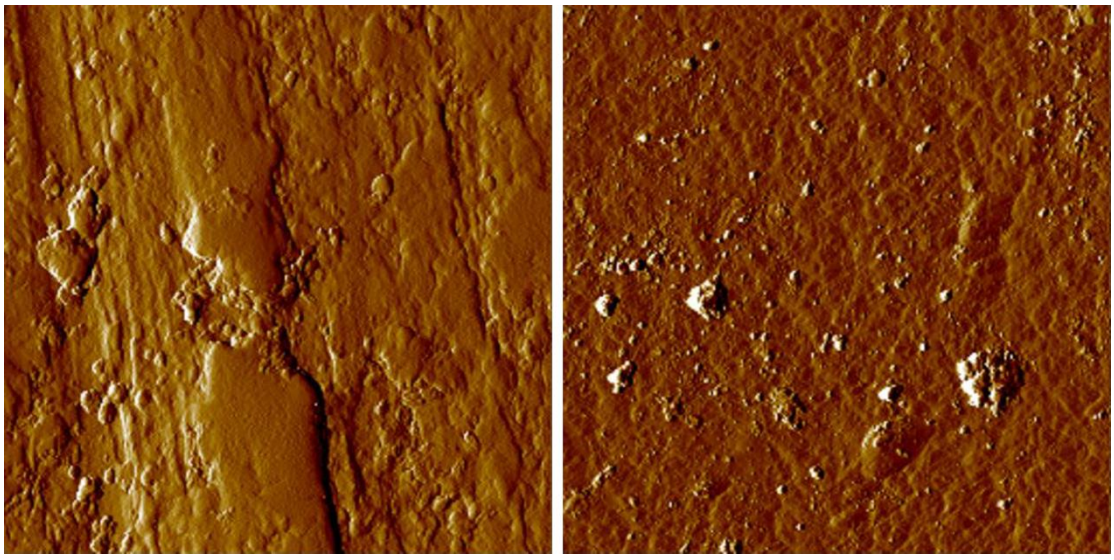

Fig. 7 AFM images of Ti6Al4V surface. (a) the original sample and (b) sample polished with 600 eV ion energy and 75 °incident angle (S14).

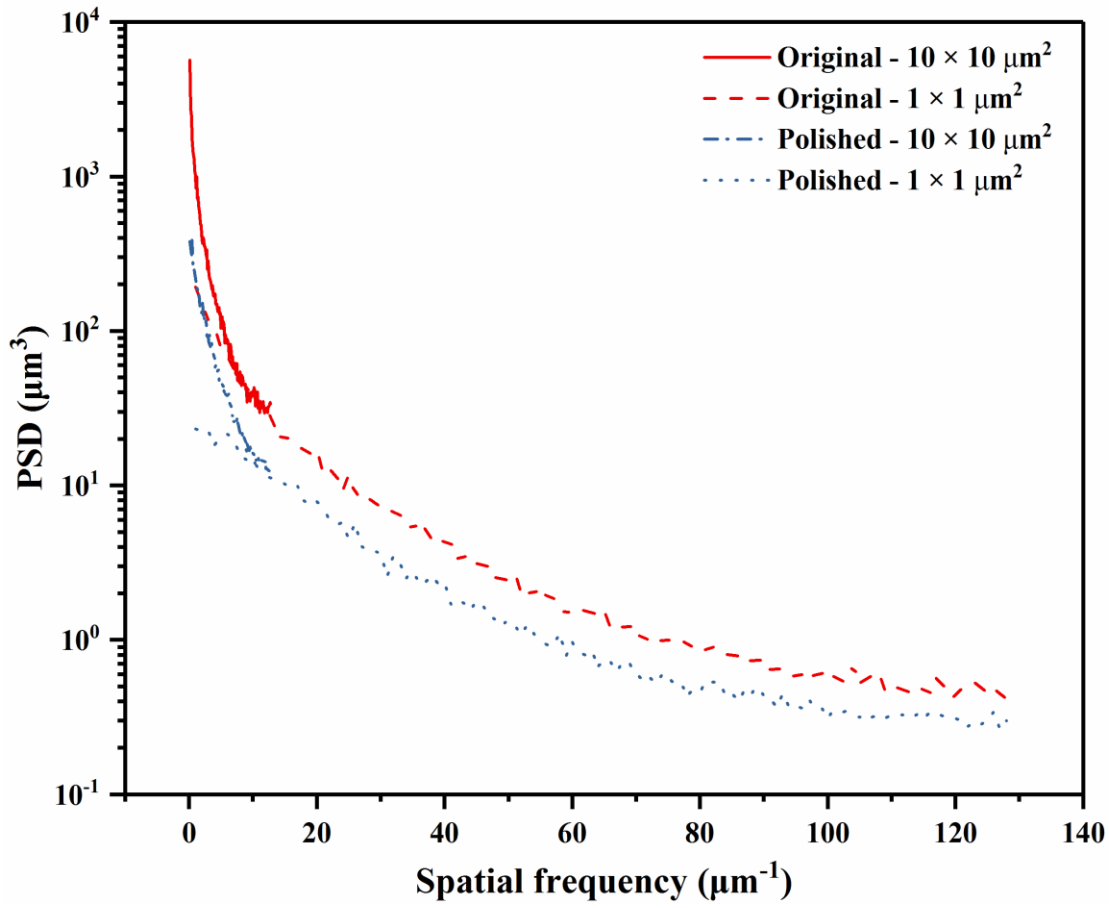

Fig. 8 PSD functions of original Ti6Al4V sample and sample polished with 600 eV ion energy and 75 °incident angle (S14).

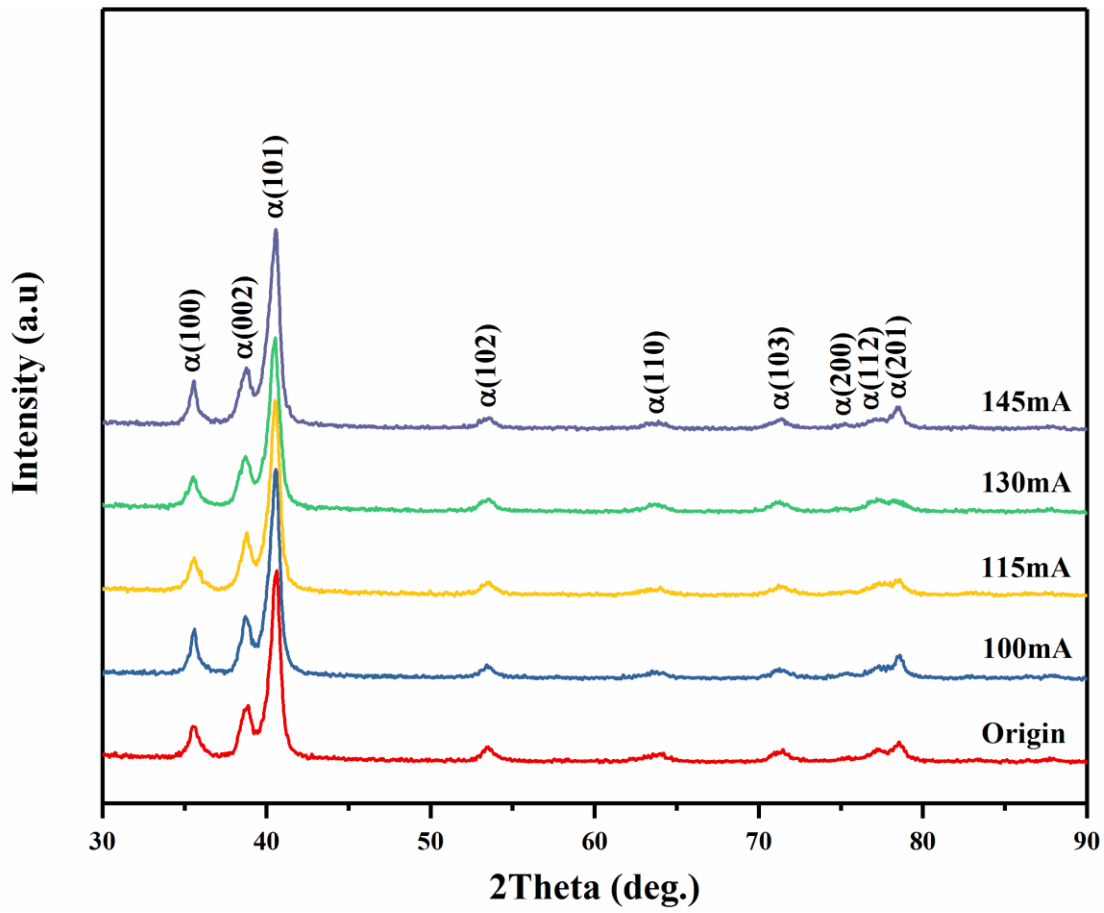
Intensity (a.u)
α(100)
α(002)
α(101)
α(102)
α(110)
α(103)
α(200)
α(112)
α(201)
145mA
130mA
115mA
100mA
Origin
30
40
50
60
70
80
90
2Theta (deg.)

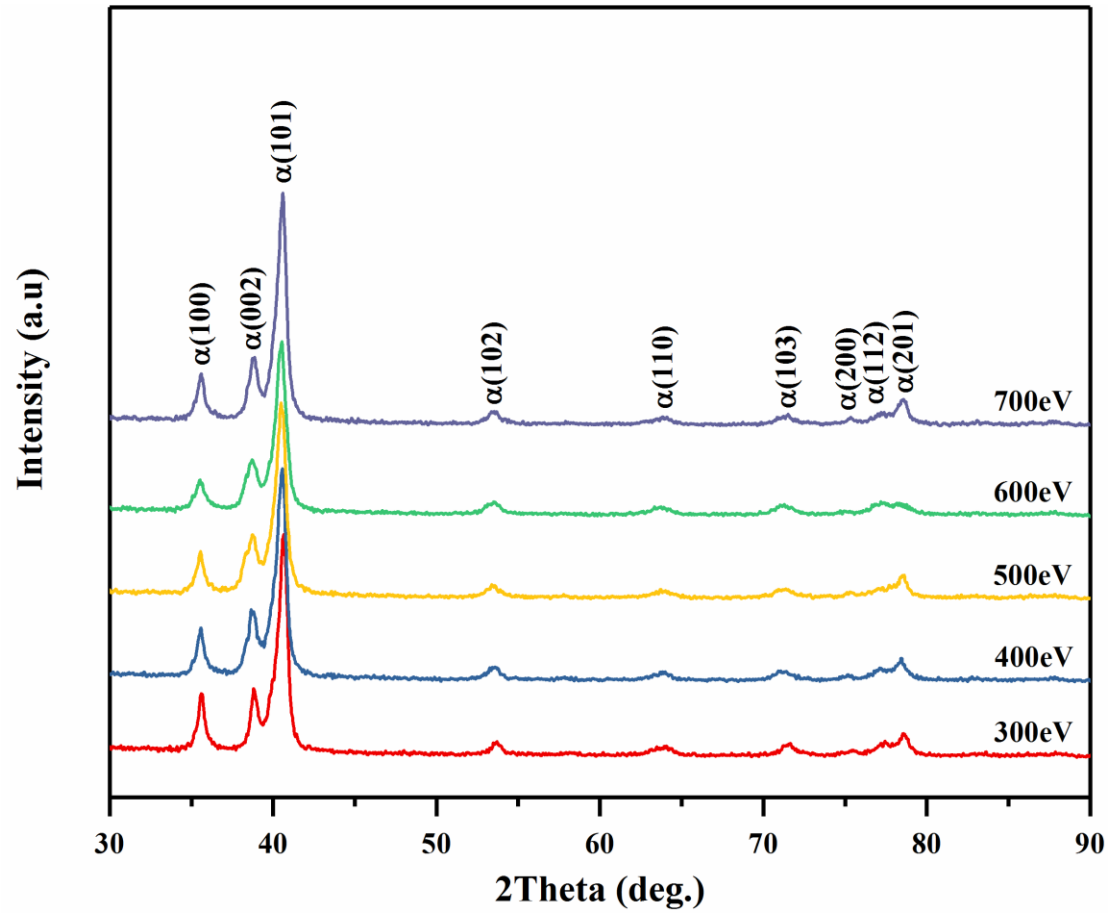

Fig. 9 GIXRD patterns of samples polished under different ion currents (a) and energies (b).

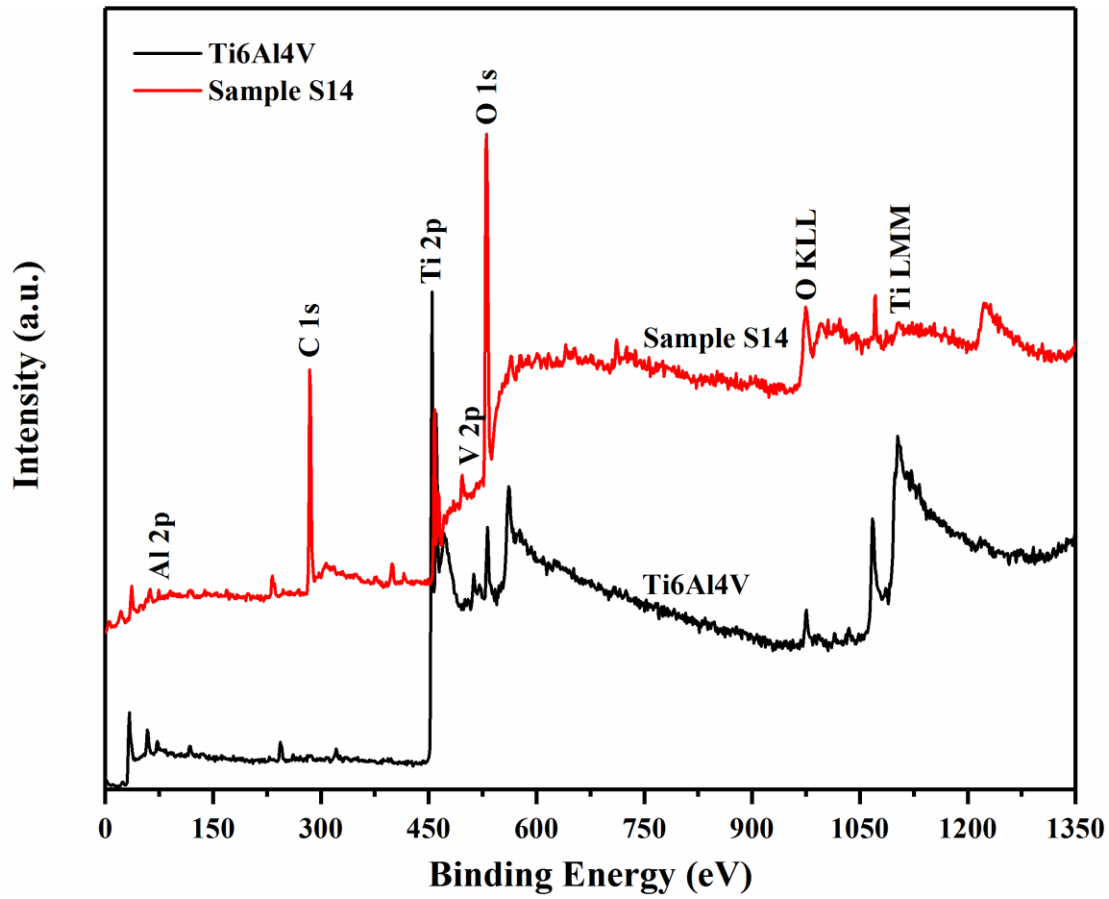

Fig. 10 XSP survey spectra of Ti6Al4V surface. (a) the original sample and (b) sample polished with 600 eV ion energy and 75 °incident angle (S14).

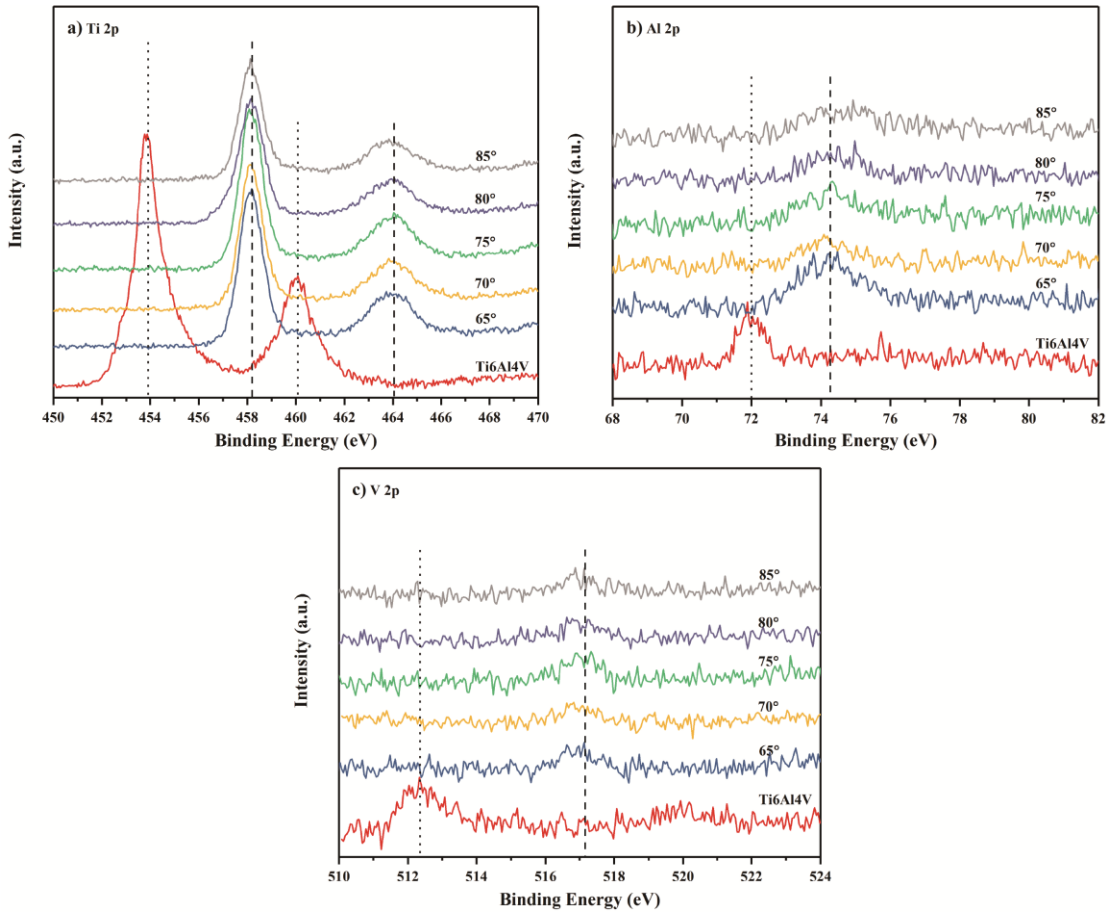

Fig. 11 High resolution XPS spectral of Ti 2p, Al 2p and V 2p for the original sample and samples polished with different ion incident angles. The dotted line represents the elements are in metallic form while the dashed line indicates that the peaks of their corresponding oxide.

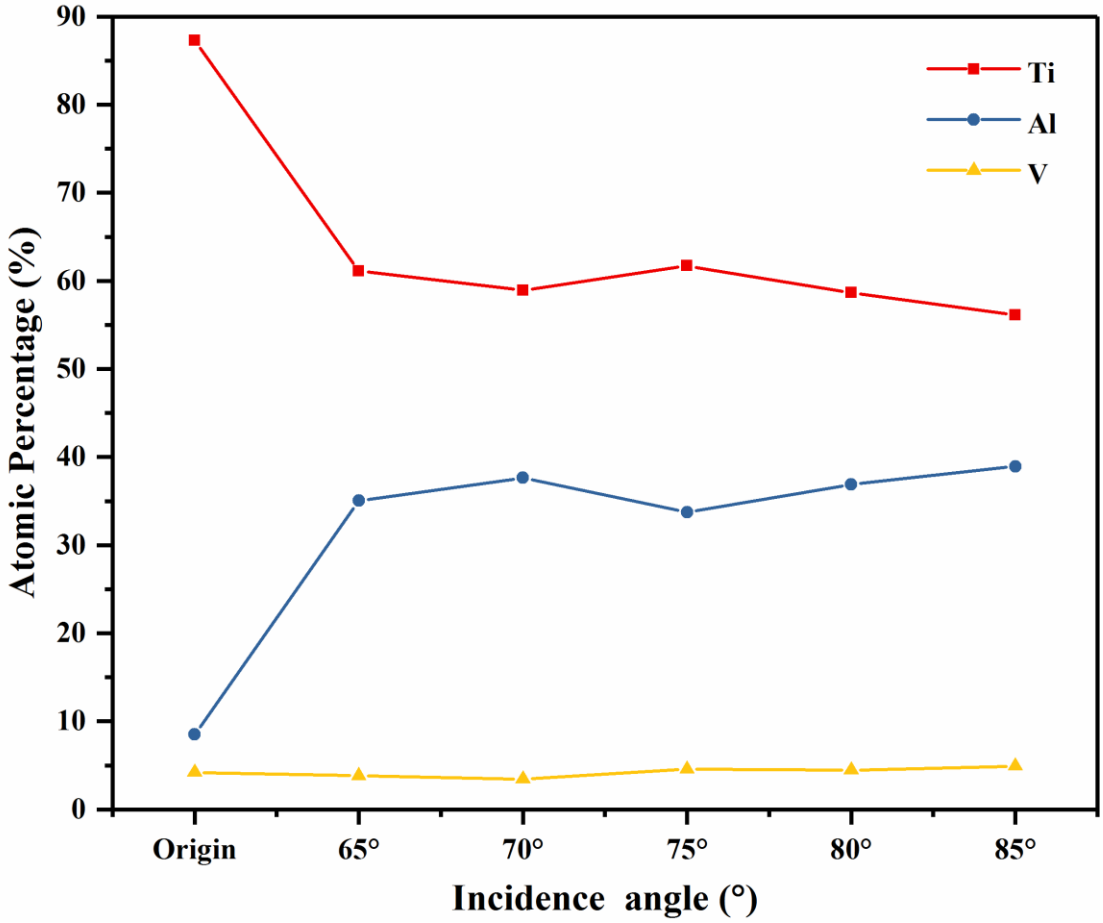

Fig. 12 Atomic percentage of the main components of Ti6Al4V for the original sample and samples polished with different ion incident angles.

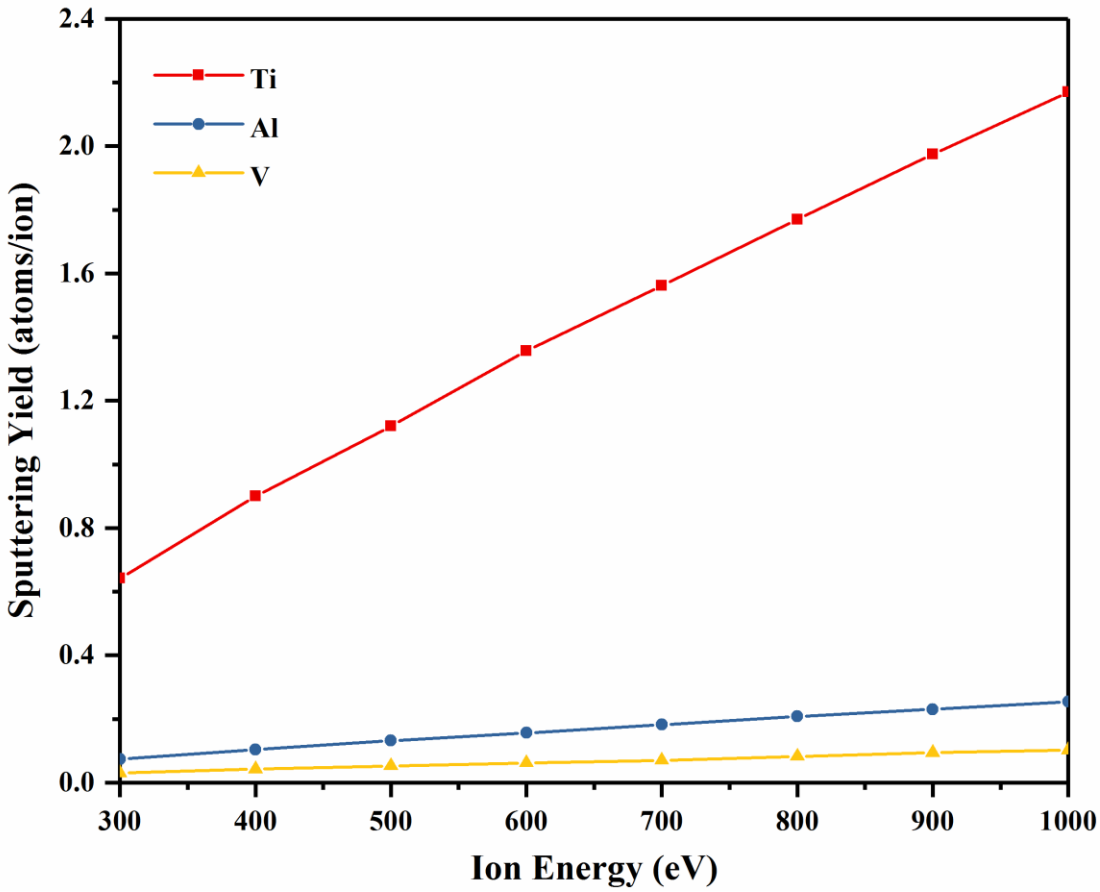

Fig. 13 Correlation between calculated sputtering yield of Ti6Al4V and ion energy at a fixed incident angle of 75 °.

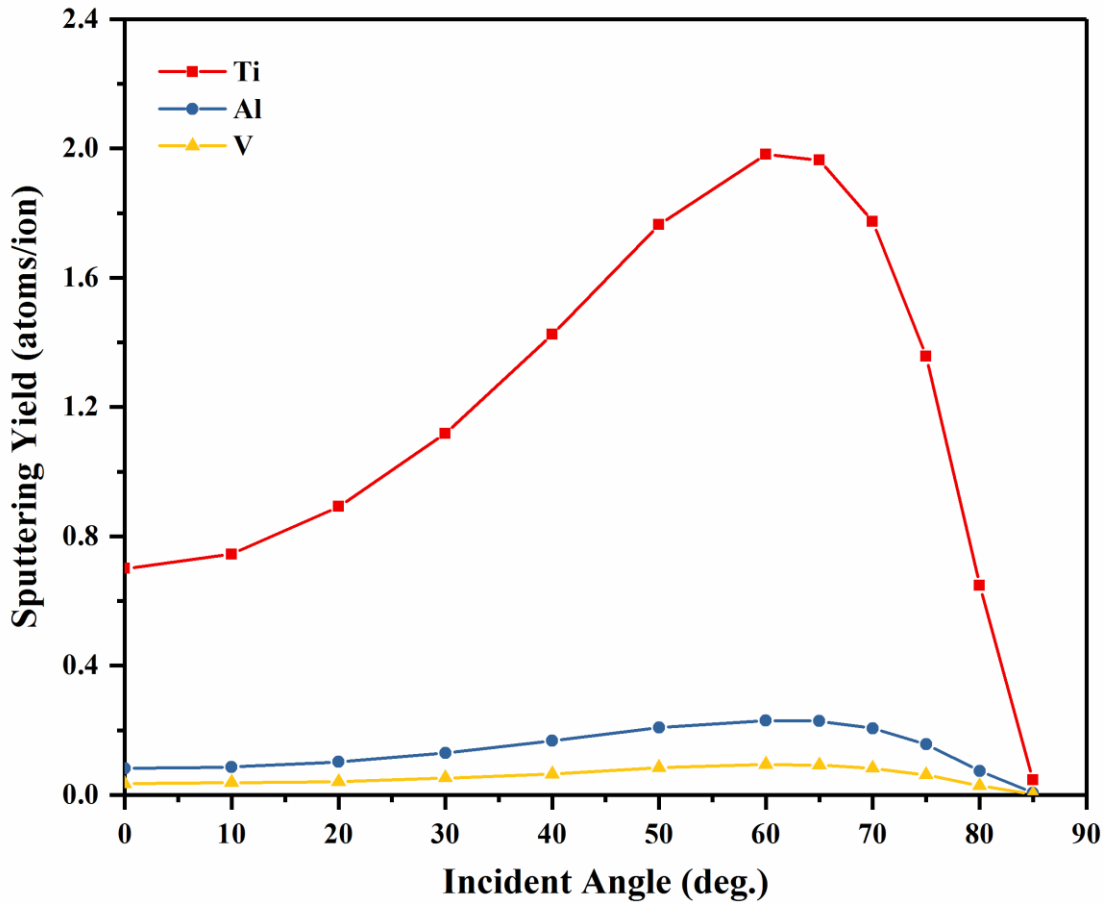

Fig. 14 Correlation between calculated sputtering yield of Ti6Al4V and ion incident angle at a fixed incident energy of 600 eV.